THE JOURNAL OF BIOLOGICAL CHEMISTRY VOL. 287, NO. 5, pp. 2948–2962, January 27, 2012

Regulation of Activity of Transient Receptor Potential Melastatin 8 (TRPM8) Channel by Its Short Isoforms*[S]

Received for publication, June 15, 2011, and in revised form, November 22, 2011 Published, JBC Papers in Press, November 28, 2011, DOI 10.1074/jbc.M111.270256

Gabriel Bidaux[‡1,2], Benjamin Beck[‡1,3], Alexander Zholos[‡4], Dmitri Gordienko[‡5], Loic Lemonnier[‡], Matthieu Flourakis[‡], Morad Roudbaraki[‡], Anne-Sophie Borowiec[‡], José Fernández[§6], Philippe Delcourt[‡], Gilbert Lepage[‡], Yaroslav Shuba[‡7], Roman Skryma[‡8], and Natalia Prevarskaya[‡8,9]

From [‡]INSERM U1003, Equipe Labellisée par la Ligue Nationale contre le Cancer, and the Université des Sciences et Technologies de Lille (USTL), F-59655 Villeneuve d'Ascq, France and the [§]Center for Vision and Vascular Science, Queen's University Belfast, BT12 6BA Belfast, United Kingdom

Background: The mechanism of regulation of ion channels often involves interaction with their nonfunctional isoforms.
Results: Cloned short isoforms of the TRPM8 cold receptor channel negatively regulate its activation mechanisms.
Conclusion: By affecting the stability of the TRPM8 C terminus, short isoforms weaken channel gating by cold and decrease its open probability (P_o).
Significance: This helps to understand the mechanisms of TRPM8 activation.

One important mechanism of the regulation of membrane ion channels involves their nonfunctional isoforms generated by alternative splicing. However, knowledge of such isoforms for the members of the transient receptor potential (TRP) superfamily of ion channels remains quite limited. This study focuses on the TRPM8, which functions as a cold receptor in sensory neurons but is also expressed in tissues not exposed to ambient temperatures, as well as in cancer tissues. We report the cloning from prostate cancer cells of new short splice variants of TRPM8, termed short TRPM8α and short TRPM8β. Our results show that both variants are in a closed configuration with the C-terminal tail of the full-length TRPM8 channel, resulting in stabilization of its closed state and thus reducing both its cold sensitivity and activity. Our findings therefore uncover a new mode of regulation of the TRPM8 channel by its splice variants.

The human genome encodes ~200 ion channels, which have been subdivided into a dozen channel families with strongly divergent structures and functional features. Members of the transient receptor potential (TRP)[10] superfamily of nonselective cationic channels display an extraordinary assortment of gating mechanisms, including some previously unrecognized modes of activation and regulation (1, 2). Almost 30 members of the mammalian TRP channel superfamily have been grouped into seven families on the basis of amino acid homologies (3). All TRP channels have six putative transmembrane domains with a pore P-loop between the fifth and sixth domains and intracellular N- and C-terminal regions of variable length (4, 5).

One of the important mechanisms of regulation of the activity of many channel types, including TRP channels, is based on the interaction of the primary (classic) isoform of the channel-forming subunit with isoforms generated by alternative splicing. Several naturally occurring splice variants of mammalian TRP channels have already been described (6, 7). In general, TRP channel isoforms may be divided into two groups depending on their structures: (i) "long" isoforms, which include most structural parts and could either form functional channels themselves (8, 9) or play the role of a dominant-negative subunit in the multimeric channel assembly (10–12) and (ii) "short" isoforms, which consist of just the N-terminal region of the full-length channel and consequently cannot form an ion permeation path but are still capable of interacting with the full-length channel and modulating its activity (6, 13). The role of these isoforms in TRP channel activation/regulation is only beginning to be understood, but it is becoming increasingly clear that this type of regulation represents an important means of altering channel biophysical properties and the physiological processes in which they are involved.

* This work was supported in part by grants from INSERM, the Ministère de l'Education Nationale, the Ligue Nationale contre le Cancer, the Agence Nationale de Recherche, the Association de Recherche sur les Tumeurs de la Prostate, and the Region Nord-Pas-de-Calais.
[S] This article contains supplemental Figs. 1 and 2 and Tables 1–3.
[1] Both authors contributed equally to this work.
[2] To whom correspondence may be addressed. E-mail: gabriel.bidaux@univ-lille1.fr.
[3] Chargé de Recherche of the FRS/Fonds de la Recherche Scientifique (FNRS). Supported by the Fondation pour la Recherche Médicale. Present address: Inst. de Recherche Interdisciplinaire en Biologie Humaine et Moléculaire (IRIBHM), 808 route de Lennik, 1070 Brussels, Belgium.
[4] Present addresses: Centre for Vision and Vascular Science, Queen's University Belfast, BT12 6BA Belfast, UK and Dept. of Biophysics, Institute of Biology, Taras Shevchenko National University of Kyiv, 01601 Kyiv, Ukraine.
[5] Supported by Derzhavniy Fond Fundamental'nikh Dosliddhzen Grant F46.2/001. Present address: Lab. of Molecular Pharmacology and Biophysics of Cell Signalling, State Key Laboratory of Molecular and Cell Biology, Bogomoletz Institute of Physiology, 01024 Kiev, Ukraine.
[6] Present address: Centre for Vision and Vascular Science, Queen's University Belfast, BT12 6BA Belfast, UK.
[7] Supported by the Visiting Scientist Program of the University of Lille. Present address: International Center of Molecular Physiology, State Key Laboratory of Molecular and Cell Biology, Bogomoletz Institute of Physiology, National Academy of Sciences of Ukraine, 01024 Kyiv, Ukraine.
[8] Both authors contributed equally to this work.
[9] To whom correspondence may be addressed. E-mail: natacha.prevarskaya@univ-lille1.fr.

[10] The abbreviations used are: TRP, transient receptor potential; sM8α, short TRPM8α; sM8β, short TRPM8β; RACE, rapid amplification of cDNA ends; EST, expressed sequence tag; eYFP, enhanced yellow fluorescent protein; eCFP, enhanced cyan fluorescent protein; LPI, lysophosphatidylinositol; PIP_2, phosphatidylinositol 4,5-bisphosphate.

TABLE 1
Primers used in this study

	Forward primers	Reverse primers	Size	Accession number
			bp	
TRPM8	5′-GATTTTCACCAATGACCGCCG-3′	5′-GAGGAGGGCATCATTATAGGAA-3′	228	AY328400
sTRPM8				
Full-length	5′-CTCAGGGAGGACTTGGTGAA-3′	5′-CACTCCTTGAAAGGCAGACTT-3′	722, 768	AY532375
Detection of exon 5a	5′-CTC AGG GAG GAC TTG GTG-3′	5′-TCC GTG TCG CAG GAC AGA CGT A-3′	266, 312	AY532375, AY532376
β-Actin	5′-CAGAGCAAGAGAGGCATCCT-3′	5′-GTTGAAGGTCTCAAACATGATC-3′	210	NM_001101

In this work, we focused on the regulation of the cold/menthol-sensitive TRP family member TRPM8 by its short splice isoforms. Although TRPM8 was originally cloned from the prostate (14), further studies have firmly established its function as a cold/menthol receptor in sensory neurons (15, 16). Because TRPM8 was also found to be up-regulated in several common human cancers, such as prostate, lung, breast, and skin, investigating possible alternatives to cold and menthol molecular mechanisms of its normal activation/regulation would lead to a better understanding of its functional significance in various tissues. Here, we describe the cloning from prostate cancer cells of two new short TRPM8 splice variants, designated short TRPM8α (sM8α) and short TRPM8β (sM8β). We show that sM8α generates two distinct proteins, named sM8-6 and sM8-18, whereas TRPM8β generates only the sM8-6 protein. We studied the differential tissue distribution of sM8α and sM8β (sM8α/β) and show that they act as regulatory subunits of the cold/menthol-activated TRPM8 channel. The mechanism of down-regulation of TRPM8 activity by the sM8-6 isoform involves interaction with the C-terminal region of the channel and conformational stabilization of its closed state. Thus, our findings provide a new insight into the mechanisms of TRPM8 channel regulation.

EXPERIMENTAL PROCEDURES

Cell Culture—The LNCaP (lymph node carcinoma of the prostate) cell line was purchased from American Type Culture Collection, and the LNCaP C4-2 cell line was a generous gift from Dr. F. Cabon. HEK-293-based cell lines were cultured in DMEM (Invitrogen) supplemented with 10% fetal calf serum and 100 μg/ml kanamycin.

Transfection—Cells were transfected using Nucleofector technology (Lonza) as described by the manufacturer. Briefly, 1 million cells were transfected with 2 μg of total vectors and plated on polylysine-coated dishes. The ratios of vectors were 1:1 for TRPM8-TRPM8 pairs, 1:2 for TRPM8-sTRPM8 pairs, and 5:1 for TRPM8-XFP or sTRPM8-XFP pairs.

Rapid Amplification of cDNA Ends (RACE)-PCR—Splice variant extremities were cloned with SMART RACE-PCR (Clontech) following the manufacturer's procedures except for the polymerases. Briefly, total mRNA from LNCaP cells were digested with DNase I for 15 min prior to phenol/chloroform purification. After ethanol precipitation of the mRNA, first-strand cDNAs were synthesized with PrimeScript reverse transcriptase from 2 μg of mRNA. RACE-PCR was performed with Phusion polymerase (Finnzymes) for 35 cycles. After PCR mixture cleanup on columns (NucleoSpin extract II, Macherey-Nagel GmbH), nested-PCR was performed on 1 μl of RACE-purified DNAs with Phusion polymerase. Amplicons were visualized on agarose gel with SYBR Green on a Dark Reader blue light table (Ozyme). After recovery of bands, DNA was recovered with NucleoSpin extract II. Terminal adenylation of DNAs was then performed with *Taq* gold polymerase prior to cloning of PCR products with pGEM-T Easy vector (Promega). Colonies were controlled by EcoRI digestion, and positive clones were submitted to sequencing.

Analysis of TRPM8 and sM8α/β mRNA Expression—Total RNA isolation, cDNA synthesis, and PCR protocols were described previously (8). Semiquantitative PCR assays were carried out under non-saturating conditions: 35 cycles for TRPM8 and 27 cycles for β-actin. Density was measured using Quantity One software (Bio-Rad). The primers used are listed in Table 1.

Cloning of sM8α/β—Specific primers based on the BE274448.1 expressed sequence tag (EST) sequence were designed and used to amplify cDNA with *Taq* gold polymerase from LNCaP mRNA, prepared as described above. Amplicons were ligated in the pCR2.1-TOPO® vector (Invitrogen). After PCR screening, clones were subjected to sequencing. Both TRPM8 splice variants were then inserted either into pcDNA3 (Invitrogen) to generate a stably expressing HEK-293 cell line or into the pCMV4-FLAG vector for transient transfection.

Fluorescent Fusion Protein Construction—A set of enhanced yellow (eYFP) and cyan (eCFP) fluorescent protein-tagged proteins was constructed for use in the FRET studies. eYFP and eCFP from peCFP-N1, peYFP-N1, and peYFP-C1 vectors were fused to the C terminus of sM8 (sTRPM8α-CFP, sTRPM8α-YFP, sTRPMb-CFP, and sTRPMb-YFP) and the TRPM8 channel (TRPM8Ct-CFP and TRPM8Ct-YFP), in addition to an N-terminal YFP fusion to TRPM8 (YFP-NtTRPM8). Fusions were realized by mutating either the stop codon (sM8 isoforms and TRPM8) or the ATG codon (TRPM8) by PCR with *Pfu* polymerase (Promega). Specific restriction sites were added to PCR primers in-phase with ORFs of fluorescent proteins. Finally, the PCR products were digested with BglII and BamHI for sM8 isoforms, NheI and XhoI for 3′-TRPM8, and XhoI and XbaI for 5′-TRPM8, followed by agarose gel purification and DNA recovery using a kit from Promega. Ligation of the open dephosphorylated vector with an insert was performed overnight at 4 °C with T4 ligase (Promega) prior to transformation in JM109 chemocompetent bacteria. The final plasmids were extracted for sequencing.

Western Blot Experiments—Total protein extraction, SDS-PAGE, and immunoblotting were performed as described (26). After blocking, membranes were soaked in 1:2000 anti-TRPM8 primary antibody (Abcam), 1:1000 anti-GFP antibody (Abcam), and 1:500 anti-actin antibody (NeoMarkers) in 2.5%

Tris/NaCl/Tween buffer/milk at +4 °C overnight. After washing several times, the strips were transferred to horseradish peroxidase-linked anti-mouse IgG secondary antibodies (Chemicon) diluted in TNT/milk (1:20,000) for 1 h. After washing several times, the strips were processed for chemiluminescence detection using SuperSignal West Dura chemiluminescent substrate (Pierce).

Immunoprecipitation Assays—Total proteins were extracted radioimmune precipitation assay buffer without SDS. 500 μg to 1 mg of proteins were incubated with 1 μg of anti-His antibody (Invitrogen) for 2 h at room temperature in 850 μl of phosphate buffer (NaH_2PO_4/NaCl). Protein A-coupled agarose beads were added and incubated overnight on a wheel at +4 °C. After three PBS washes and bead precipitation by centrifugation for 2 min at 12,000 × *g*, the supernatant was resuspended in 2× Laemmli buffer and heat at 95 °C for 5 min. Protein expression was then assessed by Western blotting and compared with the total protein extract.

Biotinylation Assays—TRPM8 cell surface expression was analyzed in a stable TRPM8-expressing HEK cell line cotransfected with either empty vector pcDNA3 or pcDNA3-sTRPM8α or pcDNA3-sTRPM8β. After 48 h, cells were washed twice with ice-cold PBS (pH 8.0) containing 1 mM $MgCl_2$ and 0.5 mM $CaCl_2$ and subjected to cell surface biotinylation. Briefly, cells were incubated for 30 min at 4 °C with 0.5 mg/ml NHS-LC-LC-biotin (Pierce) prior to two washes with ice-cold PBS (pH 8) containing 1 mM $MgCl_2$ and 0.5 mM $CaCl_2$ (PBSB) containing 0.1% (w/v) bovine serum albumin and one wash with PBS (pH 7.4) without Ca^{2+} or Mg^{2+}. Cells were homogenized in 1 ml of lysis buffer and subjected to immunoblotting as described above (see "Western Blot Experiments").

Confocal Imaging and FRET—HEK-293 cells were electroporated with an appropriate pool of vectors encoding eYFP- or eCFP-fused TRPM8 chimeras in addition to the 5′-FLAG-tagged sM8 isoforms. FRET experiments were performed with sensitized emission analysis (supplemental Fig. 1) on living cells to determine the FRET frequency (*f*(FRET)) and apparent efficiency (E_a) or with acceptor photobleaching on cells fixed with 4% formaldehyde to confirm the E_a calculation (data not shown). Confocal imaging was performed using a confocal laser scanning microscope (LSM 780, Carl Zeiss MicroImaging GmbH) with a Plan Apochromat 40×/1.3 numerical aperture oil immersion objective and equipped with a thermocontrolled chamber. A laser line of 405 nm was preferred to one of 458 nm to limit acceptor bleed-through. The acquisition procedure was standardized: 2% 405 nm laser power, 0.5% 514 nm laser power, both gains at 850, offsets at 0, pinhole opening at a 0.8-μm confocal slide, and range of CFP light collection from 430 to 494 nm because FRET and YFP ranges were from 527 nm and 661 nm. 1024 × 1024 pictures were acquired line by line with an averaging of 4 and took ~30 s to be complete. We assumed that this scanning time and averaging would limit the nonspecific FRET due to movement freedom of a cytosolic protein when studied with a membrane channel. Once the acquisition parameters had been fixed, we used them for all experiments. Zen software (Carl Zeiss MicroImaging GmbH) was used to analyze average fluorescence intensities in determined regions of interest (supplemental Fig. 1).

The E_a was quantified as the ratio of sensitized emission divided by F_{YFP} with the formula: $E_a = (F_{FRET} - F_{CFP} \times R_{CFP} - F_{YFP} \times R_{YFP})/F_{YFP}$. Positive E_a values confirmed the presence of FRET and were used to determine *f*(FRET): *f*(FRET) = number of positive FRET cells/total cells. Apparent energy transfer efficiency (E_d) was calculated in acceptor photobleaching experiment as follows: $E_d = 1 - (F_{bpb}/F_{apb})$, where F_{bpb} is CFP intensity before photobleaching and F_{apb} is CFP intensity after photobleaching.

Control experiments were performed, and constants were determined and are reported in supplemental Table 1. TRPM8-CFP chimera pairing with sTRPM8-YFP were not used, as the control pair TRPM8-CFP/YFP displayed a significant FRET frequency, which can be attributed to a local advantageous acceptor/donor ratio ([YFP] > [CFP]), producing a false positive. Indeed, a random distribution of YFP soluble protein may be able to quench the limited four TRPM8-CFP tetramer due to their higher concentration and their ability to pass through the CFP emission angle. On the other side, the TRPM8-YFP/CFP pair did not show any significant *f*(FRET), as the local acceptor/donor ratio was disadvantageous ([YFP] < [CFP]) and would then either generate a false negative or exclude the weakest FRET signal. In that case, randomly distributed CFP would still have to be well angled to transfer its energy to the YFP tetramers, and the proximity would have to be maintained along scanning. We chose the latter to keep only the true FRET signal. Pixel-by-pixel analyses were performed with ImageJ software (http://rsbweb.nih.gov/ij/) with the ImageJ plug-in "FRET and Colocalization Analyzer."

Electrophysiology and Solutions—In all cell types, membrane currents were recorded in the whole-cell configuration with the patch-clamp technique using a computer-controlled EPC-9 amplifier (HEKA Electronik) as described previously (27). Single-channel currents were recorded at room temperature (22–25 °C) using 5–7-megohm patch pipettes and an Axopatch 200B voltage-clamp amplifier (Molecular Devices). For cell-attached recordings, the resting potential was brought close to 0 mV by bathing cells with 145 mM external K^+ (*e.g.* in the extracellular solution with NaCl replaced by KCl). Currents were filtered using the four-pole low-pass Bessel filter of the patch-clamp amplifier at 2 kHz and were sampled at 10 kHz. Single-channel transitions were identified on the basis of the half-amplitude threshold crossing criteria and were analyzed using the pCLAMP 9 software.

Calcium Microfluorometry—Calcium microfluorometry experiments were performed as described previously (28). Briefly, the cytosolic Ca^{2+} concentration ($[Ca^{2+}]_i$) was measured using the ratiometric dye Fura-2 and is reported as f/f_0. The bath solution was the same one used to record TRPM8 currents.

Data Analysis—Each experiment was repeated at least three times, and the results are expressed as the mean ± S.E. Data were analyzed and graphs were plotted using Origin 5.0 software (MicroCal, Northampton, MA). InStat 3 (GraphPad Software, San Diego, CA) was used for statistical analysis, and mean values were compared using either an unpaired *t* test with Welch's correction (two groups) or one-way analysis of vari-

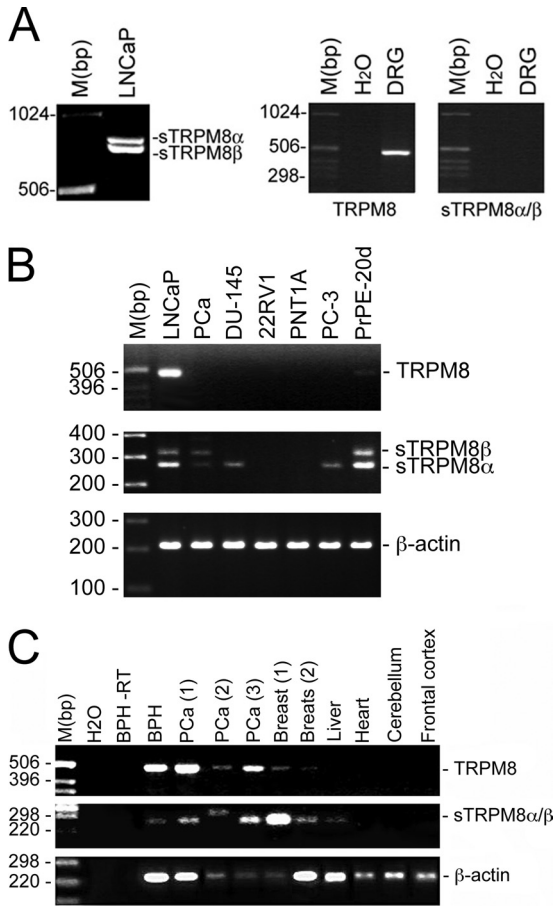

FIGURE 1. **Cloning and expression of short TRPM8 splice variants.** *A–C*, short TRPM8 splice variant (sM8α, 768 bp; and sM8β, 722 bp) mRNA amplification in the LNCaP cell line (*A*, *left panel*) and dorsal root ganglion (*DRG*) neurons (*A*, *right panel*); in human prostate cell lines (LNCaP, DU-145, 22RV1, PNT1A, and PC-3) and in primary cultures from androgen-independent prostate cancer (*PCa*) and from normal prostate after 20 days of culture (*PrPE-20d*) (*B*); and in the indicated normal human tissues, benign hyperplasia of the prostate (*BHP*) tissue, and three androgen-dependent prostate cancer (*PCa*) tissue specimens (*C*). *RT*, without reverse transcriptase.

ance with Dunnett's multiple-comparison post hoc test (three or more groups).

RESULTS

Metastatic Human Prostate Cell Line LNCaP Expresses Full-length TRPM8 and Two Shorter Splice Variants—The human *TRPM8* gene occupies the 2q37.1 position on chromosome 2 and consists of 27 exons that span >100 kilobase pairs. We previously demonstrated that the full-length TRPM8 protein is functionally expressed in the endoplasmic reticulum membrane of LNCaP cells. By analyzing the EST database, we identified one EST (accession number BE274448.1; see supplemental Table 2) that matched the sequence of the *TRPM8* gene. Based on these ESTs, we conducted RACE-PCR experiments as described under "Experimental Procedures" to detect 5′- and 3′-boundaries prior to cloning the splice variants. Two different PCR products of 722 and 768 bp (Fig. 1*A*) were specifically detected in LNCaP cells but not in a human dorsal root ganglion mRNA pool and termed short TRPM8α and TRPM8β splice variants (sM8α for the 722-bp sequence (accession number AY532375) and sM8β for the 768-bp sequence (accession number AY532376)).

EST database screening revealed that either sM8β alone or both sM8α and sM8β were expressed in colon tumor, melanoma, prostate, and endometrial adenocarcinoma cell lines (supplemental Table 1). For comparison, full-length TRPM8 was also detected in small cell lung carcinoma, choriocarcinoma, and normal liver. The EST location in the *TRPM8* genomic sequence meant that separate detection of sM8α/β expression was not possible in these samples. A series of PCR experiments validated the sM8α/β expression fingerprints (Fig. 1, *B* and *C*). We detected only sM8β in prostate cancer cells, suggesting that its expression may appear specifically during the malignant transformation of prostate cells.

Overexpression of recombinant constructs consisting of fused sM8α or sM8β and eYFP cDNAs (using the sM8 Kozak sequences) in HEK-293 cells confirmed that each splice variant coded for proteins. Surprisingly, as detected by Western blotting (Fig. 2*A*, *upper panel*), expression of the sM8α-YFP chimera resulted in two proteins, the expected 46.26-kDa protein and an additional 33.55-kDa protein, whereas expression of sM8β-YFP generated the dominant 33.55-kDa fusion protein and the minor 46-kDa protein. As depicted in Fig. 2*B*, this can be explained by the fact that both the first and third ATG codons (in exons 5b and 7a, respectively) were likely functional in sM8α and initiated the translation of a 18.66- and a 5.94-kDa native protein. In view of the complexity of the expression pattern, we will refer to the sM8α/β protein isoforms as sM8-6 (for the 5.94-kDa protein) and sM8-18 (for the 18.66-kDa protein), whereas the short TRPM8 splice variants (RNA) will be referred to as sM8α and sM8β. Because, in the sM8β splice variant, only the fourth ATG codon (exon 7a) was significantly functional, initiating the translation of 96% of the 5.94-kDa protein (Fig. 2*A*, *lower panel*), whereas the 18.66-kDa protein was virtually undetectable in Western blot experiments, we assumed that the sM8β splice variant coded only for the sM8-6 protein.

Analysis of genomic sequences revealed that the first exon of both splice variants corresponds to a new alternating exon (labeled "exon 3") of the *TRPM8* gene, which is skipped in the classic TRPM8 mRNA (Fig. 2*C*). Hence, the sM8α/β splice variants could likely be transcribed from an alternate promoter upstream of this third exon. In addition, the last exon (exon 7) of both transcripts apparently consists of two sequences: the first one (exon 7a) is part of the classic TRPM8, whereas the second represents the partial sequence of the adjacent *TRPM8* gene intron 7, now referred to as exon 7b. Integration of exon 7b most probably results from a change in splicing site recognition, preventing the use of the donor splicing site at the end of exon 7a. Exon 7b contains a putative premature stop codon, responsible for termination of the short TRPM8 protein isoforms. Finally, the only difference between the two short TRPM8 splice variants is the presence of a premature splicing acceptor site in intron 4, which generates an insertion of 46 bp in the sM8β transcript. As shown in Fig. 2*C*, we defined the parts of exon 5 as exon 5a (specific to sM8β) and exon 5b (present in short TRPM8 and sM8 isoforms). We therefore postulated that insertion of exon 5a induced skipping of the first functional ATG codon in exon 5b, thus inhibiting the translation of sM8-18 (Fig. 2*C*). This type of protein splicing mecha-

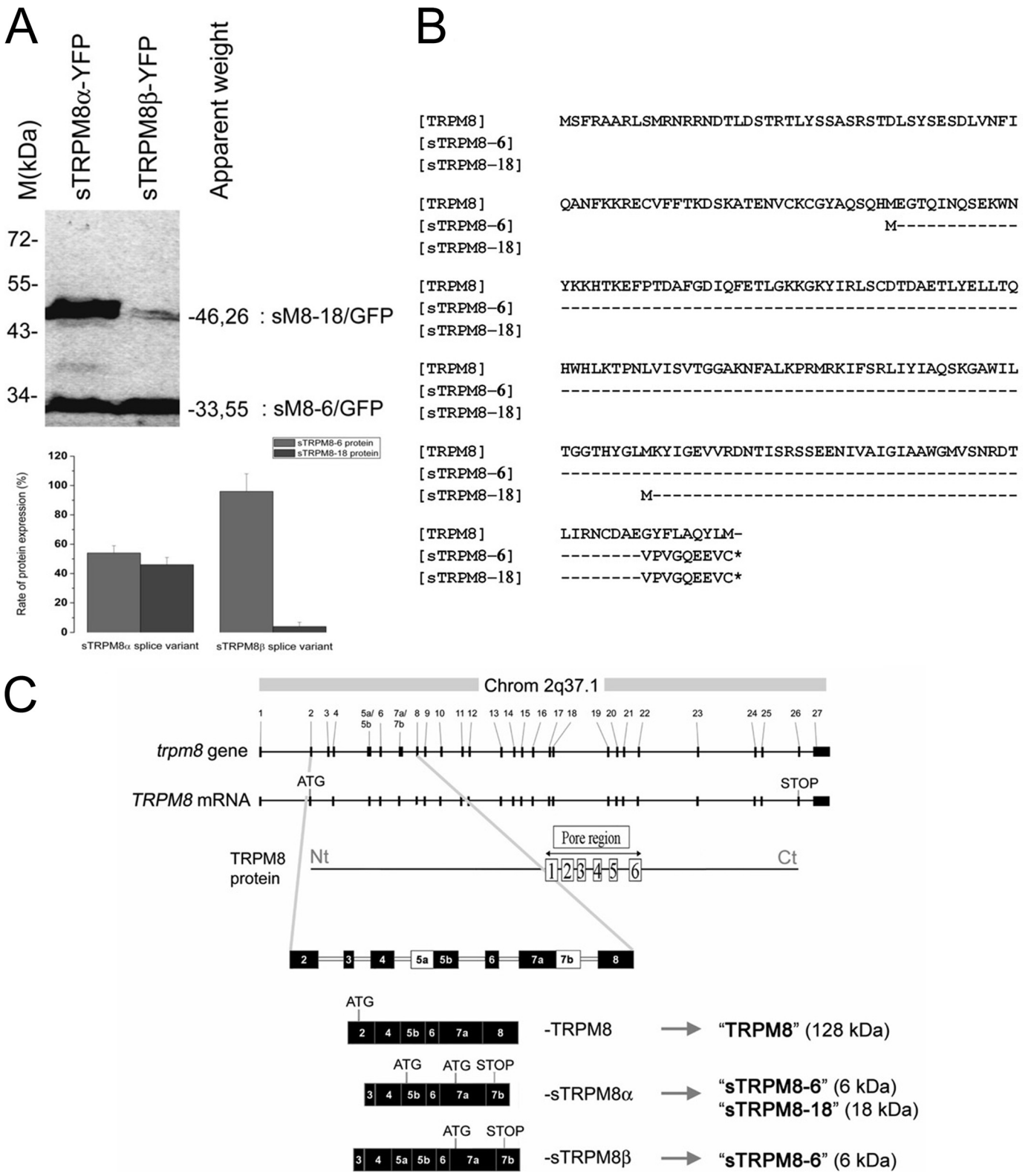

FIGURE 2. **Basic structural analysis of short TRPM8 isoforms.** *A*, *upper panel*, Western blot detection of YFP-fused short TRPM8 proteins expressed in HEK-293 cells. Splice variant α was detected in two YFP-fused forms 46.26 and 33.55 kDa in size, whereas splice variant β was detected mainly as a single 33.55-kDa form. The 27-kDa band represents free YFP used as a transfection control. *Lower panel*, quantification of protein expression. *B*, alignment of partial TRPM8 amino acid sequence with deduced amino acid sequences of both sM8α and sM8β (accession numbers AAZ73614.1, AAS45275.1, and AAS45276.1, respectively). *C*, at-scale genomic organization of the *TRPM8* gene and full-length TRPM8 mRNA aligned with secondary protein structure. The *three lower plots* show not-to-scale organization with numbered exons of partially homologous regions of TRPM8 (accession number DQ139309), sM8α (not-to-scale; accession number AY532375), and sM8β (not-to-scale; accession number AY532376) mRNAs. Exons 5 and 7 include two acceptor and two donor sites for alternative splicing, respectively. Therefore, exon 5 was divided into exons 5a and 5b, as exon 7 consists of exons 7a and 7b. The ATG and STOP codons are shown for each protein. *Chrom*, chromosome; *Nt*, N terminus; *Ct*, C terminus.

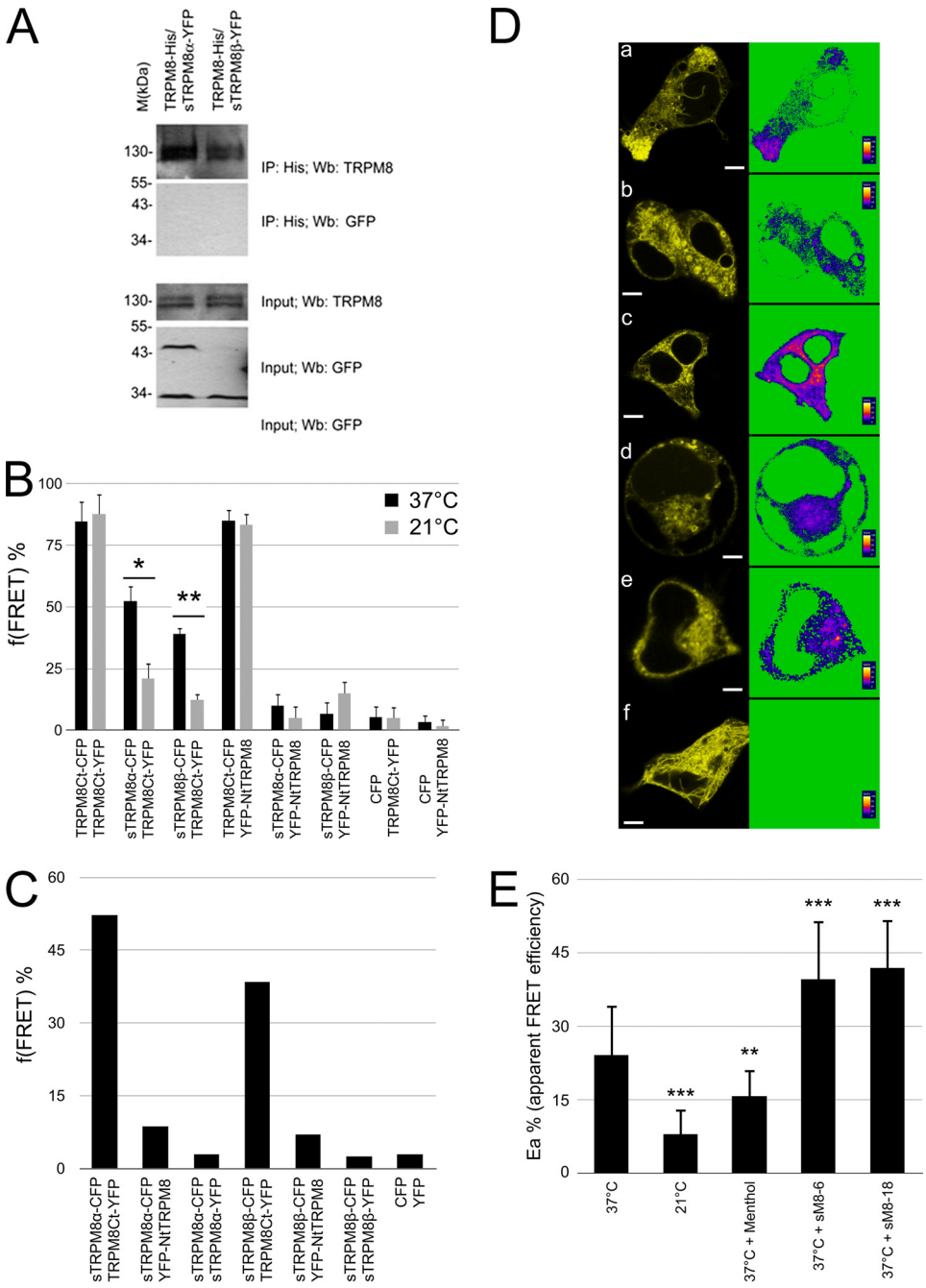

FIGURE 3. **sM8 isoform-TRPM8 relationship.** *A*, immunoprecipitation (*IP*) of His-tagged TRPM8 protein followed by immunoblotting with anti-GFP antibody failed to detect sM8 isoforms (*upper panels*). Input experiments detected the TRPM8 protein as well as the sM8-6 and sM8-18 isoforms (*lower panels*). YFP was used alone as a negative control. *Wb*, Western blot. *B*, averaged *f*(FRET) (three independent experiments) at 37 and 21 °C for the indicated pairs of CFP- or YFP-labeled proteins heterologously coexpressed in HEK-293 cells (see "Experimental Procedures" for details and supplemental Table 3). *C*, *f*(FRET) calculated from three combined sets of experiments. *D*, pixel-by-pixel mapping of the apparent FRET efficiency in living cells transfected with the following pairs: *panel a*, M8Ct-M8Ct at 37 °C; *panel b*, M8Ct-M8Ct at 21; *panel c*, M8Ct-M8Ct at 37 °C with FLAG-tagged sM8-18; *panel d*, M8Nt-M8Ct at 37 °C; *panel e*, M8Ct-sM8a at 37 °C; and *panel f*, M8Nt-sM8a at 37 °C. *Scale bars* = 5 μm. *E*, averaged apparent FRET efficiency between TRPM8Ct-YFP and TRPM8Ct-CFP in living cells depending on the external temperature, the addition of 500 mM menthol, or cotransfection of the sM8-6 and sM8-18 isoforms. Cell numbers for each condition are 31, 31, 21, 20, and 25, respectively. Statistical significance is indicated as follows: *, $p < 0.05$; **, $p < 0.01$; ***, $p < 0.001$.

nism is well known and could be essential for generating short TRP isoforms (17).

Interaction of Short TRPM8 Isoforms with C-terminal Loop of Full-size TRPM8 Channel Is Thermosensitive—The potential interaction between full-size TRPM8 and its short isoforms was investigated by co-immunoprecipitation and FRET. As demonstrated in Fig. 3*A*, none of the short TRPM8 isoforms coprecipitated with full-size TRPM8, which is consistent with a recent study demonstrating that the N-terminal peptides of TRPM8 do not precipitate with the full-length protein (18). Thus, we investigated the thermosensitivity of this hypothetical interaction, which could explain why coprecipitation failed to detect it.

FRET confocal analysis was following a sensitized emission protocol and confirmed by acceptor photobleaching to deter-

mine the proximity among TRPM8 C and N termini within the tetrameric channel assembly and the proximity between sM8 isoforms and the TRPM8 channels. After calibration of microscope settings, controls were performed, and constants were calculated (see "Experimental Procedures" and supplemental Table 1). HEK-293 cells were cotransfected with different combinations of plasmids containing full-size TRPM8 fused with either eYFP or eCFP and FLAG-sM8α/β (at a respective ratio of 1:1:4). FRET experiments were conducted on living cells at either 37 or 21 °C, and sensitized emission was assessed to confirm FRET. FRET frequency (*f*(FRET)) was calculated as described under "Experimental Procedures." As shown in Fig. 3*B*, at 37 °C, FRET was detected between C-terminal extremities of TRPM8 (M8Ct) and between the N-terminal extremity (M8Nt) and the M8Ct extremity at a frequency of ~80% for both cases (*i.e.* 85 ± 12% and 85 ± 2%, respectively). In addition, neither *f*(FRET) was affected by cooling to 21 °C (88 ± 8% and 83 ± 5%, respectively), which is known to activate the TRPM8 channel. FRET was also detected between sM8α-M8Ct and sM8β-M8Ct at 52 ± 12% and 39 ± 9%, respectively, but not for sM8α-M8Nt and sM8β-M8Nt, indicating close proximity between sM8 and the C-terminal extremity of TRPM8. Furthermore, experiments conducted at 21 °C demonstrated a sizable decrease in FRET between sM8α-M8Ct and sM8β-M8Ct to 21 ± 6% and 12 ± 3%, respectively, suggesting that cooling results in their detachment. As M8 C termini are known to be highly interactive through their coil-coiled domains (18) and because the *f*(FRET) of M8 C termini was found to be insensitive to cooling, the reversal of the proximity between sM8 and M8 cannot be explained by the movement of M8Ct, but more likely results from the movements of the short TRPM8 isoforms. Indeed, unbound sM8 can randomly and quickly change the CFP angle of emission and/or move out of the field, consequently decreasing the YFP quenching. Furthermore, neither sM8α-M8Nt and sM8β-M8Nt nor eCFP-M8Ct and eCFP-M8Ct displayed any significant FRET.

As the sM8 isoforms are homologous to the N-terminal loop of TRPM8, one would expect that they can interact with each other, as has reported for interacting homodomains. Thus, we postulated that if sM8 sequence represents the minimal unit of a putative homodomain, we would detect a FRET signal between two sM8 isoforms or between sM8 and M8Nt, whereas a lack of FRET between sM8 and M8Nt would indicate too long of a distance between the homologous domains on the N-terminal loop and the N-terminal extremity. We then carried out respective experiments, and as shown in Fig. 3*C*, we did not detect any meaningful *f*(FRET) between sM8α-sM8α and sM8β-sM8β compared with eCFP-sM8α and eCFP-sM8β or eCFP-eYFP.

Short Isoforms Counteract Conformational Changes to TRPM8 C Termini during Channel Activation—Single-cell pixel-by-pixel analysis and average FRET efficiency were calculated and then averaged for FRET-positive cells. Fig. 3*D* shows that activation of the TRPM8 channel by cooling to 21 °C drastically decreased FRET between C termini, whereas the presence of either sM8-18 or sM8-6 shifted FRET efficiency to higher levels. Indeed, the averaged apparent energy (E_a) at 37 °C (24 ± 10%) showed a significant decrease in FRET between TRPM8 C termini when activating TRPM8 with 500 μM menthol (16 ± 5%) or by cooling to 21 °C (8 ± 5%). As C termini tetramerize via their extreme coil-coiled domains, one can conclude that menthol-induced TRPM8 activation and, even more so, cold-induced TRPM8 activation either take apart C termini or rotate C-terminal extremities such that YFP and CFP turn away from each other, decreasing YFP ability to quench the CFP signal, which can be interpreted as a conformational change. Both sM8-6 and sM8-18 isoforms induced a significant increase in E_a (to 40 ± 12% and 42 ± 10%, respectively), indicating that either the C termini became closer or the relative position between CFP and YFP altered in the opposite way to that occurring during TRPM8 activation.

In conclusion, the results of our FRET experiment strongly suggested that short TRPM8 isoforms interact with the C terminus of the TRPM8 channel and that this interaction is temperature-dependent. Moreover, we demonstrated that TRPM8 activation triggers a conformational change in the tetrameric assembly of C termini that has a functional outcome opposite the one induced by short isoforms. Therefore, we hypothesized that sM8 stabilizes the C terminus of TRPM8, leading to a more stable closed conformation.

Short TRPM8 Isoforms Negatively Regulate Activity of TRPM8 Channel and Define Its Responsiveness to Menthol and Cold—We used a combination of electrophysiology and $[Ca^{2+}]_i$ microfluorometry to characterize the putative regulation of "classic" TRPM8 channel activity by short isoforms. Fig. 4*A* shows averaged $[Ca^{2+}]_i$ responses of TRPM8-transfected HEK-293 cells (HEK-M8/Ctrl cells) loaded with Fura-2/AM to the application of cooling compounds (menthol or icilin) known to be TRPM8 agonists. Coexpression of TRPM8 with either the sM8α (HEK-M8/sM8α cells) or sM8β (HEK-M8/sM8β cells) splice variant resulted in a marked decrease in the menthol-induced and lysophosphatidylinositol (LPI)-induced calcium signals (Fig. 4*A*). However, the icilin-induced signal was not modified by sM8β expression but was slightly decreased in the presence of sM8α.

In patch-clamp experiments, exposure of HEK-M8/Ctrl cells to cold (21 °C), menthol (500 μM), and icilin (10 μM) activated the TRPM8-mediated membrane current (I_{TRPM8}) with characteristic prominent outward rectification and a reversal potential close to 0 mV (Fig. 4*B*). It is noteworthy that the currents induced by menthol and cold had much higher densities (236.0 ± 30.9 and 222.9 ± 4.1 pA/picofarads, respectively, at +100 mV) compared with the icilin-induced current (94.5 ± 10.3 pA/picofarads) under identical experimental conditions. Coexpression of sM8β resulted in the inhibition of both cold- and menthol-evoked currents but slightly increased the icilin-induced current (Fig. 4, *C* and *D*). Specific overexpression of the FLAG epitope-tagged sM8-6 protein confirmed that the effect of the sM8β splice variant was carried solely by the sM8-6 isoform (Fig. 4*D*). Intriguingly, sM8-6 isoform expression resulted in a marked potentiation of the icilin-evoked current, confirming the tendency observed with sM8β transfection in patch-clamp experiments. Coexpression of sM8α also inhibited the TRPM8-mediated current (Fig. 4*E*). However, in this case, two nearly equal populations of HEK-M8/sM8α cells were clearly distinguishable. In the first population, cold-, menthol-, and

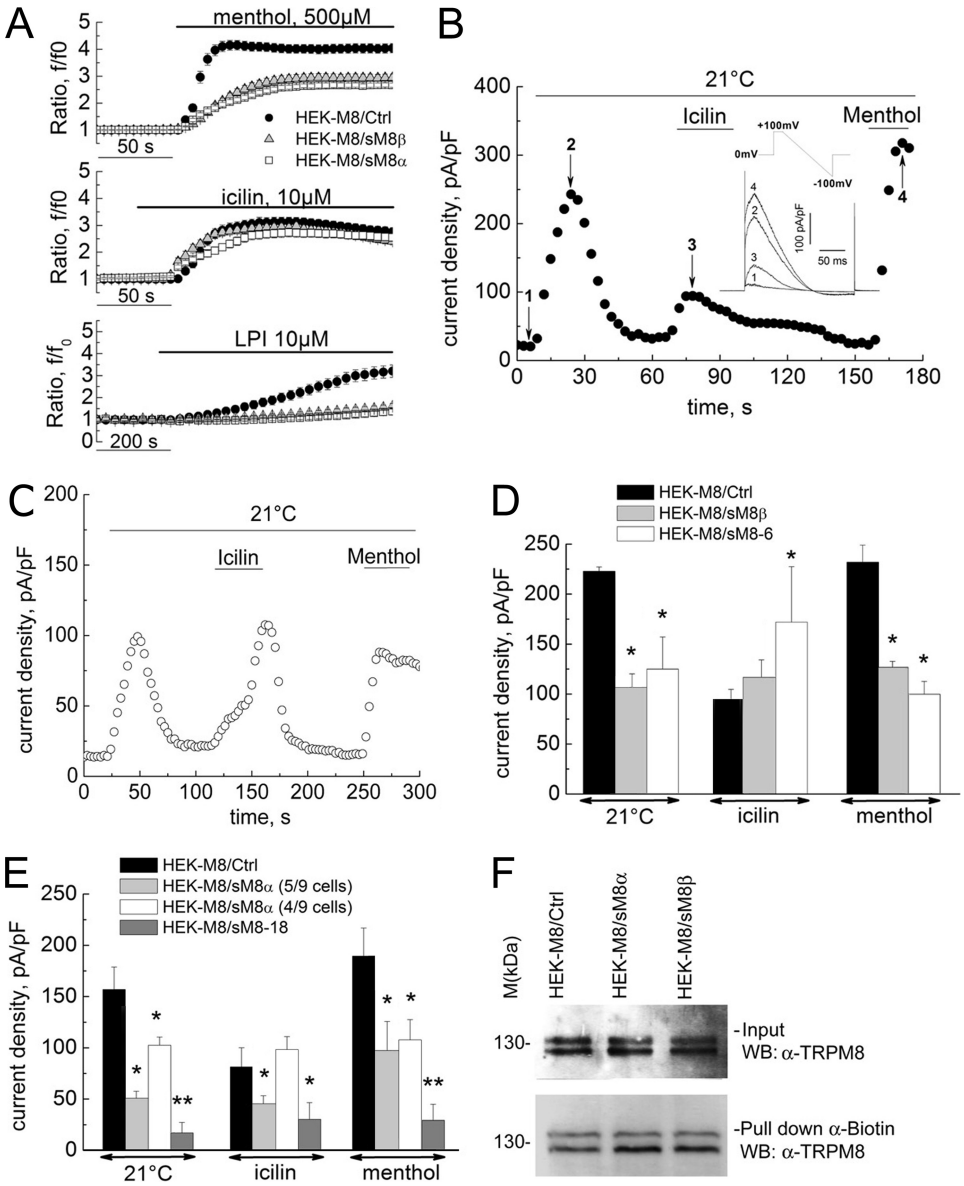

FIGURE 4. **Functional effect of sM8 isoform expression on TRPM8-mediated responses.** *A*, averaged time courses of cytosolic Ca^{2+} (expressed as the f/f_0 ratio; mean ± S.E.) in response to menthol (500 μM; *upper panel*), icilin (10 μM; *middle panel*), and LPI (5 μM; *lower panel*) in control HEK-M8/Ctrl cells (*closed circles*; $n = 108$), HEK-M8/sM8α cells (*open squares*; $n = 105$), and HEK-M8/sM8β cells (*shaded triangles*; $n = 111$). *B*, changes in membrane current density measured at +100 mV in representative HEK-M8/Ctrl cells exposed to cold (21 °C), menthol (500 μM), and icilin (10 μM), as indicated by *horizontal bars*. The *inset* shows superimposed raw currents in response to a voltage-ramp pulse protocol between +100 and −100 mV, acquired at the time points marked by the *numbers* on the time course. *pF*, picofarad. *C*, same as in *B* but for a representative HEK-M8/sM8β cell. *D*, comparison of maximum current densities (mean ± S.E.) activated by menthol, icilin, and cold in HEK-M8/Ctrl cells (*black bars*; $n = 42$), HEK-M8/sM8β cells (*gray bars*; $n = 64$), and HEK-M8/sM8-6 cells (*white bars*; $n = 31$) *, significant difference ($p < 0.01$). *E*, same as in *D* but comparing HEK-M8/Ctrl cells (*black bars*), HEK-M8/sM8α cells (*light gray* and *white bars*), and HEK-M8/sM8-18 cells (*dark gray bars*). Two cell populations were distinguished in this case based on icilin response: five of nine cells showed potent inhibition of all responses, including icilin, by sM8α coexpression (*light gray bars*), whereas four of nine cells showed smaller inhibition of cold- and menthol-activated currents and no inhibition of the icilin-induced current (*white bars*), similar to HEK-M8/sM8β cells. Statistical significance is indicated as follows: *, $p < 0.05$; **, $p < 0.01$. *F*, Western blot (*WB*) showing TRPM8 detection after cell surface biotinylation in HEK-M8/Ctrl, HEK-M8/sM8α, and HEK-M8/sM8β cells. *Upper panel*, total protein extract; *lower panel*, proteins pulled down with streptavidin beads ($n = 3$).

icilin-evoked currents were inhibited, exactly as in HEK-M8 cells overexpressing the sM8-18 isoform (Fig. 4*E*). In the second population, cold- and menthol-evoked currents were inhibited, but the icilin-evoked current was slightly potentiated (Fig. 4*E*), as was observed in the case of sM8-6 isoform overexpression (Fig. 4*D*). Finally, no change in phosphatidylinositol 4,5-bisphosphate (PIP_2)-dependent rundown of the TRPM8-mediated current was detected with either sM8-18 or sM8-6 coexpression, suggesting that short isoform-dependent TRPM8 modulation is PIP_2-independent (supplemental Fig. 2, *A* and *B*).

To investigate whether variations of I_{TRPM8} in the presence of short isoforms are associated with differential plasmalemmal TRPM8 targeting, Western blot detection of TRPM8 after cell surface biotinylation was performed. Fig. 4*F* shows that, in fact, both sM8-6 and sM8-18 isoforms slightly increased translocation of the full-length TRPM8 protein to the plasma membrane (to 130 ± 27% ($p < 0.01$) and 141 ± 25% ($p < 0.05$) of the control, respectively). These data rule out the decreased membrane expression as a mechanism underlying the observed inhibitory effects but may explain the sM8-6-dependent increase in icilin-evoked I_{TRPM8}.

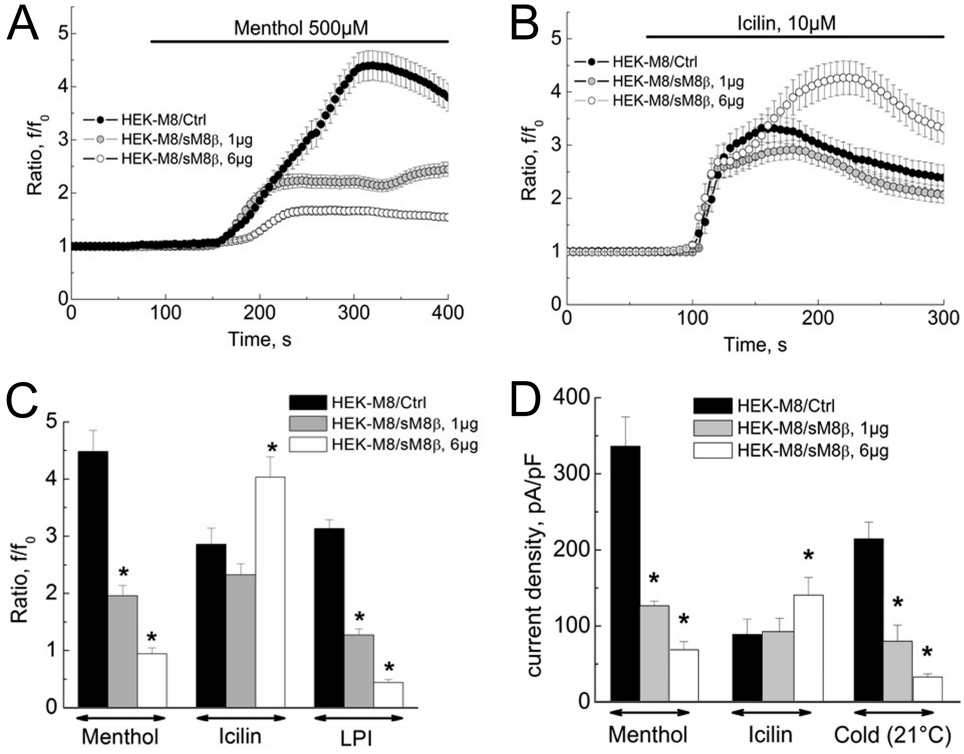

FIGURE 5. **Dose dependence of sM8β effects.** *A* and *B*, averaged time courses of cytosolic Ca^{2+} (expressed as the f/f_0 ratio; mean ± S.E.) in response to menthol (500 μM; *A*) and icilin (10 μM; *B*) in control HEK-M8/Ctrl cells (*closed circles*; $n = 118$) and in HEK-M8/sM8β cells transfected with 1 μg (*shaded circles*; $n = 118$) or 6 μg (*open circles*; $n = 118$) of sM8β plasmid. *C*, comparison of maximum $[Ca^{2+}]_i$ responses (measured as the f/f_0 ratio; mean ± S.E.) to menthol (500 μM) and icilin (10 μM) in HEK-M8/Ctrl cells (*black bars*; $n = 118$) and HEK-M8/sM8β cells transfected with 1 μg (*gray bars*; $n = 118$) or 6 μg (*open bars*; $n = 118$) of sM8β plasmid. *D*, comparison of maximum current densities (mean ± S.E.) activated by menthol (500 μM), icilin (10 μM), and cold in HEK-M8/Ctrl cells (*black bars*; $n = 10$) and HEK-M8/sM8β cells transfected with 1 μg (*gray bars*; $n = 12$) or 6 μg (*open bars*; $n = 14$) of sM8β plasmid. *, statistically significant ($p < 0.05$). *pF*, picofarad.

To determine the dose dependence of short isoform action on the classic TRPM8 channel, cells were cotransfected with different ratios of sM8α/β and TRPM8 cDNAs. Our results clearly demonstrate that the higher concentration of sM8β cDNA (6 μg/ml) was more potent in inhibiting the menthol-induced $[Ca^{2+}]_i$ increase (~80% inhibition) than the lower concentration (1 μg/ml, ~60% inhibition) (Fig. 5*A*). However, although sM8β at a lower concentration was unable to modify the icilin-evoked $[Ca^{2+}]_i$ increase, at a higher concentration, it even enhanced it (to 141.2 ± 12.3% of the control) (Fig. 5*B*).

The major difference in the concentration dependence of sM8β effects on menthol-, LPI-, and icilin-evoked Ca^{2+} signals (Fig. 5*C*) was further confirmed by patch-clamp recordings on the same batches of cells (to avoid batch-to-batch variability) (Fig. 4*D*): a high level of sM8β expression decreased both menthol- and cold-activated currents by ~80% in contrast to the icilin-activated current, which was increased by ~50% (Fig. 5*D*). The sM8β-induced shift in TRPM8 channel menthol and cold sensitivity indicates that, in the given cell, it strongly depends on the quantitative ratio of the expression of the full-size and short isoforms. This could also explain the discrepancy in sM8-6 and sM8β vector effects on TRPM8-mediated calcium influx and TRPM8 current (Fig. 4, *A* and *D*), as sM8-6 is an N-terminal FLAG-tagged fusion construct using the Kozak consensus sequence for initiation of translation, whereas sM8β is a C-terminal GFP-fused chimera using the endogenous sM8 Kozak sequence that is far from the consensus. In addition, these data highlight that sM8 efficiency with respect to both cold- and menthol-induced TRPM8 currents is less dependent on the quantity of sM8 (1.3-fold increase for both stimuli) compared with the icilin-induced current, which was enhanced by 4.9-fold. A direct correlation between the amount of sM8β and the amplitude of the icilin-evoked current emphasizes the putative role of sM8 isoforms in the translocation of full-size TRPM8 to the plasma membrane.

To determine whether short isoforms act like a "lure" for menthol or modulate TRPM8 activity irrespective of menthol binding, we carried out dose-effect patch-clamp measurements for menthol. As no significant variations in the EC_{50} value for menthol-evoked I_{TRPM8} in the presence of sM8β were detected, we concluded that modulation of TRPM8 channel activity by short isoforms does not involve interference with ligand binding.

Short TRPM8 Isoforms Modify Temperature Dependence of Open Channel Probability—Previous studies demonstrated that activation of TRPM8 and some other temperature-sensitive TRP family members involves temperature-dependent shift in the channel's voltage-dependent activation (19). We therefore investigated whether short isoforms influence the voltage dependence of TRPM8 gating by comparing steady-state current activation curves in HEK-M8/Ctrl, HEK-M8/sM8α, and HEK-M8/sM8β cells acquired using a standard tail current protocol (Fig. 6*A*) as described previously (19, 20). Experimental data points were fitted to the sigmoid Boltzmann

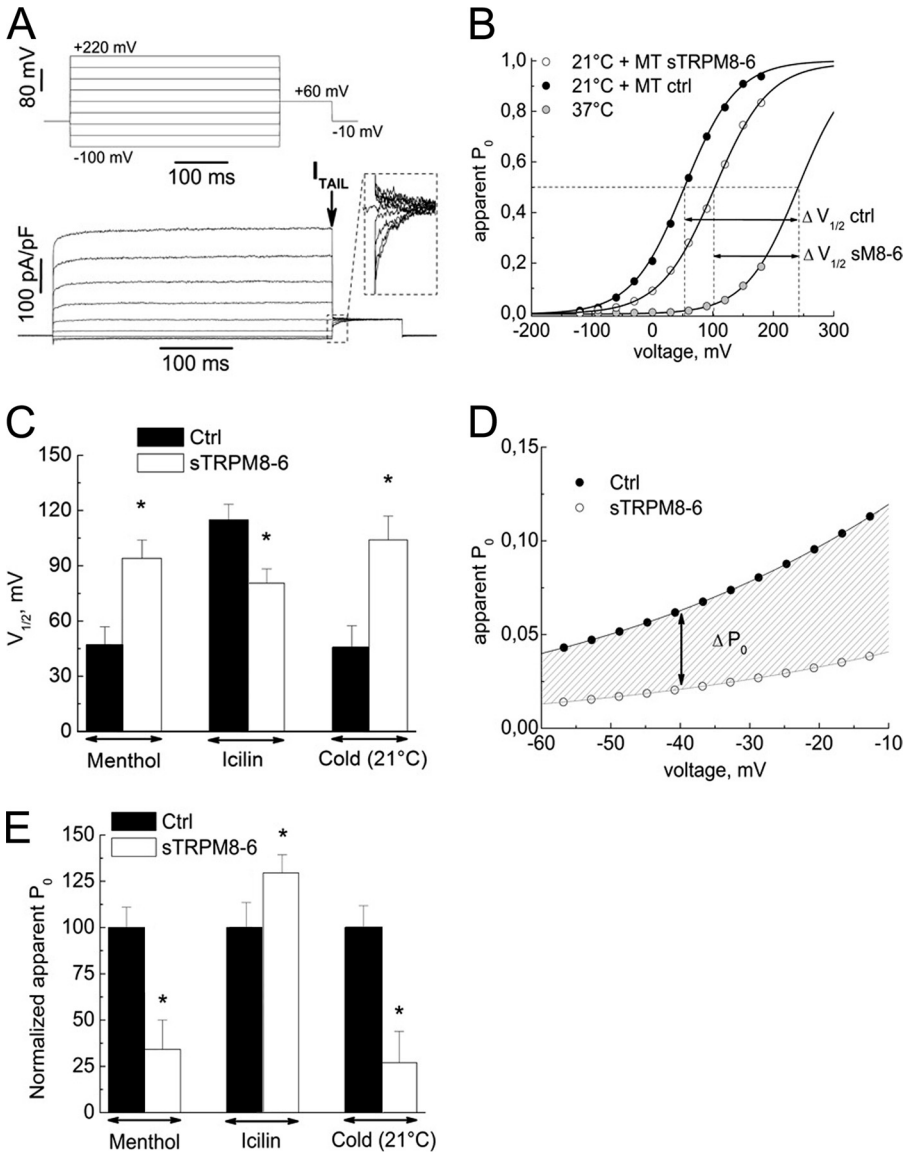

FIGURE 6. **Effects of sM8-6 coexpression on TRPM8 channel voltage dependence and heat sensitivity.** *A*, raw currents in response to the indicated voltage-clamp protocol in the representative HEK-M8/Ctrl cell exposed to menthol (500 μM) used to measure the apparent P_o based on the amplitude of current tails (shown in the *inset*). The tail current (I_{TAIL}) was measured at the time indicated by the *arrow*. *B*, voltage dependence of TRPM8-mediated current activation (apparent P_o *versus* voltage) in HEK-M8/Ctrl cells at 37 °C (*gray circles*) and 21 °C in the presence of menthol (*MT*; 500 μM) in HEK-M8/Ctrl cells (*ctrl*; *closed circles*); coexpression of the sM8-6 protein caused a depolarizing shift in current activation in response to cold (21 °C) and menthol (500 μM) (*open circles*). The *solid lines* represent the best fit of experimental data points with the Boltzmann equation; the *dashed lines* indicate the respective values of $V_{1/2}$. *C*, comparison of $V_{1/2}$ values for TRPM8-mediated current activation (mean ± S.E.) in the presence of menthol (500 μM), icilin (10 μM), or cold (21 °C) in HEK-M8/Ctrl cells (*Ctrl*; *black bars*; $n = 32$) and following coexpression of the sM8-6 protein (*white bars*; $n = 47$). *D*, magnified view of the dependences in *B* for the "physiological" range of resting potentials to present physiologically relevant differences in the voltage dependence of TRPM8 activation conferred by sM8-6 (*hatched area*). *E*, comparison of TRPM8 activation levels (mean ± S.E.) at −40 mV in the presence of menthol (500 μM), icilin (10 μM), or cold (21 °C) without (*Ctrl*; *black bars*; $n = 32$) or with (*open bars*; $n = 47$) sM8-6 coexpression. Apparent P_o values were normalized to the values in HEK-M8/Ctrl cells. *, statistically significant ($p < 0.05$).

equation (Fig. 6*B*) to derive the following activation parameters: the half-maximum activation voltage ($V_{½}$) and the slope factor (s), proportional to the gating charge.

Comparison of the steady-state activation dependences of cold-activated I_{TRPM8} revealed a depolarizing shift of nearly 50 mV in $V_{½}$ associated with sM8-6 coexpression (from 40.0 ± 9.9 mV in HEK-M8/Ctrl cells to 104.1 ± 14.9 mV in HEK-M8/sM8β cells) (Fig. 6, *B* and *C*, respectively). A shift of nearly the same magnitude was also observed for menthol-activated I_{TRPM8} (Fig. 6*C*). However, consistent with our previous results, sM8-6 coexpression had the opposite effect on the steady-state activation of the icilin-evoked current, producing a hyperpolarizing shift in $V_{½}$ from 115 ± 8.4 mV in HEK-M8/Ctrl cells to 80.5 ± 7.8 mV in HEK-M8/sM8β cells. The sM8-6-related shift in $V_{½}$ for menthol- and cold-activated currents toward positive values reduced the apparent open probability (P_o) of the channel at physiological potentials (*i.e.* around −40 mV) by 3-fold (Fig. 6*D*), in contrast to icilin, with which the P_o actually increased by 30% (Fig. 6*E*). This indicates a considerably suppressed cold-induced inward current at the physiological potentials.

Single-channel Insights into Action of Short TRPM8—We next asked what changes in the biophysical characteristics of

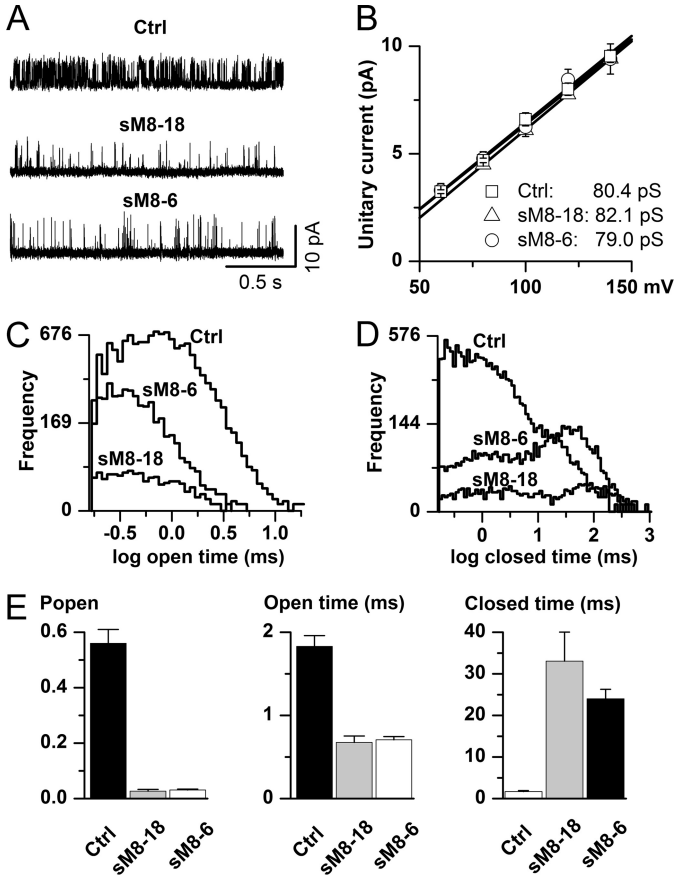

FIGURE 7. **Ion channel mechanism underlying inhibition of TRPM8 channel by short TRPM8 isoforms.** *A*, representative examples of single-channel activity recorded in the cell-attached configuration in membrane patches held at 120 mV relative to the cell resting potential. Less frequent channel openings were evident with the sM8-18 ($n = 5$) or sM8-6 ($n = 10$) isoform coexpressed with the full-length TRPM8 protein (*Ctrl*; $n = 6$). *B*, the isoforms did not alter single-channel conductance, suggesting that short TRPM8 isoforms do not cause any hindrance of the ion permeation pathway. This analysis was restricted to positive potentials only because openings were brief and likely incompletely resolved in the negative range (21). *C* and *D*, comparisons of the open (*C*) and closed (*D*) interval distributions constructed using logarithmic binning (20 bins per decade) after executing the event search algorithm of the pCLAMP 9 program. Events briefer than 0.16 ms were ignored as poorly resolvable (21). Note that the main changes occurred in the long closed component domain. In parallel, the short isoforms significantly reduced the proportion of short closings. *E*, mean data showing reduction in the channel P_o (*left panel*) accompanied by some reduction in the mean open time (*middle panel*) and a dramatic increase in the mean closed time (*right panel*) with either isoform. Statistical tests using analysis of variance with the Tukey-Kramer multiple-comparison test revealed significant differences between mean values for all measured parameters ($p < 0.0001$ in all cases), with both isoforms showing differences from the control ($p < 0.001$ in all cases) but not between themselves ($p > 0.05$ in all cases).

TRPM8 channel functioning may be responsible for the short isoform-induced decrease in TRPM8 activity. Single-channel recordings revealed a dramatic decrease in TRPM8 activity when either of the short TRPM8 isoforms was coexpressed. In HEK-M8/Ctrl cells, very frequent channel openings were observed at positive potentials and room temperature, but with both isoforms, the closed intervals became notably longer, thus dramatically reducing the frequency of channel openings (Fig. 7*A*). However, unitary conductance remained unchanged (Fig. 7*B*), indicating that alterations in channel kinetics are likely the only reason for the whole-cell current inhibition by the short TRPM8 isoforms. We recently proposed a single-channel mechanism of TRPM8 activation by membrane depolarization and cold (21). This involves transitions between at least two open and five closed states, and its full analysis in terms of the action of TRPM8 short isoforms is presented in our accompanying article (22). Briefly, we found that alteration of TRPM8 kinetics by sM8-6 isoforms involved changes that closely mimicked heat action, such that 12 of the 12 rate constants describing the seven-state model moved in the same direction by both increased temperature and coexpression of short isoforms (22). Here, we show only several of the most fundamental aspects of altered TRPM8 gating by its short isoforms. First, we found that the mean open time remained relatively unaltered (Fig. 7, *C* and *E*, *middle panel*), suggesting not only that the permeation pathway was not affected by the isoforms (in conjunction with data shown in Fig. 7*B*) but also that there was no significant interaction of the isoforms with the open conformation of the channel. Second, distributions of closed times were dramatically changed by the isoforms (Fig. 7*D*) such that normally infrequent prolonged closures became dominant with the presence of both short peptides. Such changes directly indicate preferential stabilization of the long closed conformations of TRPM8 by short isoforms. An increased frequency of the longest closed times clearly explains the significant reduction in the channel P_o (Fig. 7*E*, *left panel*), as these parameters are related. Altogether, our data demonstrate that short TRPM8 isoforms represent fine-tuned regulators of the TRPM8 channel via stabilizing its conformation in the closed state.

DISCUSSION

In this study, we identified and characterized two new short splice variants representing N-terminal TRPM8 channel fragments: sM8α and sM8β. We demonstrated that these isoforms are not simply products of mRNA degradation or mistranscription but represent complete functional proteins that may play a key role in TRPM8 channel regulation.

Intriguingly, generation of short isoforms involves both mRNA and protein splicing. Indeed, we reported that the sM8α splice variant codes for the 6- and 18-kDa protein isoforms, whereas the sM8β splice variant codes only for the single 6-kDa protein. These data highlight the complexity of the regulatory mechanisms for TRPM8 protein and gene expression.

TRPM8 acts as a thermodynamic sensor, where cooling specifically affects the stability of the channel in the closed state, as was demonstrated in our recent study (21). Studies confirmed that the rate of the closed-to-open transition is highly temperature-dependent (19, 21) due to the high activation energy required. In this respect, it is important to note that the cold-sensitive domain of TRPM8 has been traced to the C-terminal region (23). In this work, we demonstrated that the sM8-6 and sM8-18 isoforms drastically reduce menthol-, cold-, and LPI-induced I_{TRPM8} by interfering with the C terminus of the classic full-size TRPM8 channel-forming subunit, causing the decrease in channel P_o. As we were unable to detect a change in the EC_{50} for menthol or a significant shift in the half-activation temperature ($T_{1/2}$) (data not shown), we concluded that sM8 does not affect the heat sensor directly or compete with the putative menthol-binding domain on the channel. In addition,

our data show that the relative amount of sM8-6 to TRPM8 directly defines the inhibitory power of sM8-6.

Remarkably, sM8-6 expression failed to affect the voltage dependence of the P_o when icilin was used as an activating agent. Because specific amino acid residues essential for icilin activation had been traced to the TRPM8 intracellular loop connecting transmembrane domains 2 and 3 (24), this suggests that this loop is not modified by interaction with sM8-6, but it is likely that the heavier sM8-18 may interfere with this loop to decrease the icilin-induced TRPM8 activation. Indeed, the structural differences of sM8 could induce a differential effect: the longer isoform, sM8-18, not only interferes with the C terminus but also alters the opening pore of TRPM8, leading to a dominant-negative effect. On the contrary, sM8-6 would be able to interfere only with the C terminus and would not be able to directly alter the opening pore. In general, our data are consistent with the notion that short isoforms do not alter various ligand-binding sites but rather modify their allosteric coupling to the basic gating machinery of the channel. Furthermore, our data demonstrate that the 6-fold overexpression of sM8β only slightly enhanced the inhibition of both cold- and menthol-induced TRPM8 currents (by 1.3-fold) but drastically stimulated the icilin-induced current (by 4.9-fold). The significant increase in the icilin-activated TRPM8 current is most likely explained by indirect mechanisms associated with sM8 accumulation, such as promotion of TRPM8 translocation and/or decrease in TRPM8 turnover within the plasma membrane. However, the ratios of endogenous sM8 and TRPM8 mRNAs are such that these mechanisms can hardly take place in the native cells.

The C terminus of TRPM8 is known to be regulated by PIP_2, which is essential for TRPM8 activity (23, 25). Indeed, PIP_2 has been shown to suppress rundown of the TRPM8-mediated current, whereas PIP_2 depletion triggers a dramatic decrease in TRPM8 P_o. Furthermore, cooling is known to sensitize TRPM8 to PIP_2. It was therefore proposed that cooling and menthol facilitate the interaction of the C terminus with PIP_2, leading to TRPM8 activation. However, PIP_2 is equally effective in regulating TRPM8 activation by icilin. Our data demonstrate no changes in PIP_2-dependent rundown of the TRPM8 current in the presence of the sM8-6 isoform, indicating a lack of sM8-6 interference with PIP_2 sensitivity and pointing out that the sM8-6 isoform interferes with the way TRPM8 is activated upstream by a conformational shift in its cold sensor without modifying the channel's ability to sense cold and without influencing the interaction of the C terminus with PIP_2.

Surprisingly, we observed that sM8-6 interfered with TRPM8 activation by LPI. In our previous study on the modulation of TRPM8 activity by lysophospholipids, we demonstrated that LPI drastically increases the mean channel open time without changing the closed time (26). Furthermore, a recent study has shown that both menthol- and icilin-evoked TRPM8 activities are dependent on the direct interaction with LPI and lysophosphatidylethanolamine (27). Therefore, we postulated that sM8-6-mediated inhibition of TRPM8 occurs downstream of the activation by lysophospholipids.

The outstanding question is how short TRPM8 isoforms act on TRPM8 to control its activation selectively. In our FRET experiments, cooling triggered a 60% decrease in *f*(FRET) between sM8 and M8Ct. There are several hypotheses that could explain this observation, and they are discussed below.

1) sM8 free movement in the cytosol is altered by temperature. Indeed, diffusion of free molecules is faster at 30 °C than at 21 °C, indicating that a single sM8 molecule would stay longer in a position favoring FRET with M8Ct, which is opposite what we really observed. In addition, we did not detect significant FRET either between free CFP and M8Ct-YFP or between CFP and YFP-NtM8, suggesting that sM8-CFP remains in a stable position at the proximity of the TRPM8 C termini. Thus, either sM8 directly interacts with TRPM8 or is linked to TRPM8 indirectly through a TRPM8 partner. 2) Disruption of M8Ct tetramerized coil-coiled domains. This would also result in a strong decrease in *f*(FRET) between C termini, which was not the case. 3) Rotation of CFP coupled to sM8 enables YFP quenching. Because of the small size of sM8, it is unlikely that they would be able to rotate independently from each other while interacting with TRPM8 or a TRPM8 partner. Such a locked (sM8-CFP) rotation would be possible only for the free sM8 form (but see Hypothesis 1). 4) The tetramerized C termini in the *z*-axis are displaced such that C-terminal extremities would be pushed away from the pore region. This hypothesis suggests that sM8-CFP would stay in complex with either TRPM8 or the intermediate TRPM8 partner linking it to TRPM8. However, we did not detect any coprecipitation of TRPM8 and the short isoforms, indicating that they do not interact strongly enough. 5) Finally, a last probable hypothesis would be that sM8 would interact (directly or indirectly) with the C terminus of TRPM8 and that this interaction would indirectly depend on temperature. A direct reversible interaction is quite likely, as it has been reported that truncated or full-length N-terminal portions of TRPM8 are able to interact with its C terminus in a two-hybrid system but not in the immunoprecipitation assay (18).

Considering the data from this study on FRET analysis and the data from the accompanying study of unitary currents (22), we propose a model of sM8 actions (Fig. 8*A*). First, we show that during activation of the TRPM8 channel by cold and, to a lesser extent, by menthol, the C terminus undergoes conformation shifts. This agrees with Brauchi *et al.*, who concluded that (i) during TRPM8 activation with cold, the C terminus loses its hydrophobic interactions (20), and (ii) the C terminus by itself is or includes the thermosensor (23).

The two-state model of TRPM8 gating suggests that the closed state of the channel is the most stable and that cooling decreases the stability of the closed state, enabling brief transitions to the open state (19). Thus, we believe that the probability of the TRPM8 C-terminal thermosensor to change its conformation, leading to channel opening, increases with cooling. When the conformation of the C terminus shifts, detecting the cold, the whole TRPM8 structure becomes unstable and allows the pore to open.

Second, our data are consistent with the role of short TRPM8 isoforms in stabilizing the C terminus in the closed conformation. An interaction between sM8 and closed TRPM8 would explain why the channel's closed dwell time drastically increases in the presence of sM8 (22). Because the half-activa-

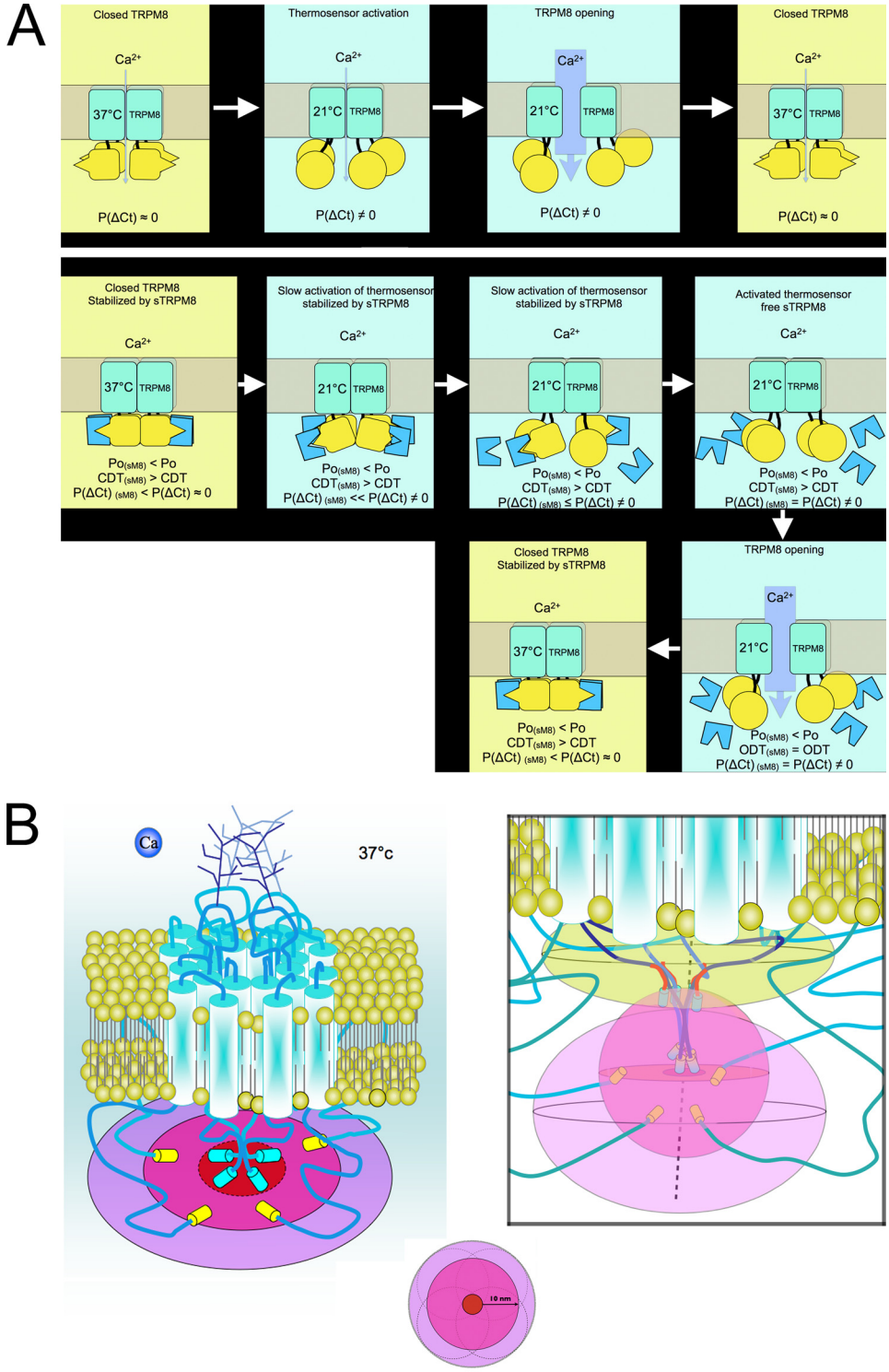

FIGURE 8. **Prediction of spatial distribution of TRPM8 extremities and sM8 isoforms.** *A*, model representing (i) cold-induced TRPM8 opening (*upper panels*) and (ii) a probable mechanism explaining the thermoreversibility of the sM8-TRPM8 interaction (*lower panels*). The C terminus of TRPM8 is shown in *yellow*, and sM8 is shown in *blue*. *P(ΔCt)* is the probability that the TRPM8 C terminus shifts its conformation. *CDT* and *ODT* are the closed and open dwell times, respectively, measured by Fernández *et al.* (22). The N termini of TRPM8 are not shown. *B*, schematic depiction of the TRPM8 channel and its extremities (N termini fused with YFP and C termini fused with CFP) within the horizontal plane (denoted by *ellipses*) crossing the tetramer of the C termini (*left panel*). The color coding of the plane is presented below and represents the spatial distribution of the C termini (*red* center area), FRET limits of the TRPM8 C termini (*pink* middle area) equal to the maximum distance of FRET efficacy (10 nm), and FRET limits of the TRPM8 N termini, hypothesizing that they are localized at ~10 nm from the C termini (*light violet* outer area). *Left panel*, possible two-dimensional layout of the TRPM8 C and N termini; *right panel*, our three-dimensional model of probabilistic volumes in which sM8 (*upper sand*-colored area), TRPM8 C termini (*middle pink*-colored area), and TRPM8 N termini (*lower light violet*-colored area) evolve. sM8 isoforms are short *red* segments coupled to CFP; TRPM8 C termini are *dark blue* segments coupled to CFP; and TRPM8 N termini are *turquoise* segments coupled to YFP.

tion temperature ($T_{1/2}$) is not affected by sM8, it seems that short isoforms make the channel more difficult to activate rather than impair its cold sensitivity. The relative constancy of $T_{1/2}$ is also consistent with the reversibility of sM8-TRPM8 FRET in response to temperature changes. Indeed, if the sM8-TRPM8 interaction had been strong and thermostable, the sM8 effect would have been a dominant-negative one and would have been expected to affect the $T_{1/2}$. In fact, we hypothesized that sM8 could interact with the TRPM8 C terminus only in its "closed conformation" equal to the "37 °C stable conformation."

The thermodynamic model of TRPM8 activation predicts that the closed state of the channel becomes progressively less stable as the temperature decreases. Our data indicate that this is accompanied by the transition of the C terminus to the conformation in which it is unable to interact with sM8 isoforms. In such a conformation, the C terminus becomes free and subject to Brownian movements. The absence of interaction between sM8 and TRPM8 during TRPM8 opening is consistent with the observation that open dwell time is not modified in the presence of sM8 (22). As soon as TRPM8 is closed, the sM8 isoforms are free to bind again to the TRPM8 C terminus. Finally, in accordance with the parsimony law, we propose that the sM8-TRPM8 relationship would likely be a direct interaction with a heterodomain, with one of its domains being thermosensitive.

FRET is a useful tool to enhance the resolution of an optical system from a conventional ~200 nm up to 10 nm. Using FRET enabled us to propose a model resolving the conformation of TRPM8 extremities as well as to uncover putative actions of sM8 isoforms (Fig. 8*B*). Note that due to steric limitations, sM8 isoforms coupled with fluorescence proteins are likely to interact within the TRPM8 C-terminal sequence located between the thermosensor and the coil-coiled domain. The presence of sM8 just beneath the pore area pushes out the N terminus in a spheroid area spanning from the horizontal plan, including C termini, to a radius of 10 nm below.

Another interesting feature revealed by the FRET analysis is the conformational shift in the tetrameric C-terminal assembly during TRPM8 activation with menthol. The conformational shift in the C termini produced by menthol appeared to be comparable in orientation but less intense that the shift that occurred during channel activation with cold, suggesting that it is a necessary requisite of agonistic action of both cold and menthol. Furthermore, we have demonstrated that short isoforms decrease the menthol-evoked current but do not change the EC_{50} for menthol. Together with previous findings showing that exchanging the C termini of TRPM8 and TRPV1 strongly reduces (by 10-fold) the menthol-activated current through TRPM8 but does not change the EC_{50} for menthol (23), our data highlight the major role of the conformational change in the TRPM8 C terminus in channel opening by cooling and menthol but not by icilin.

Finally, the physiological relevance of sM8 would need to be further investigated. An important question to be answered is how short isoforms function in native cells. Our previous study shows that TRPM8 in the LNCaP prostate cancer cell line may function not only as a plasmalemmal cationic channel but also as cold/menthol-activated endoplasmic reticulum Ca^{2+} release channel (28). Here, we did not address the issue of the regulation of the endoplasmic reticulum-localized TRPM8 by sM8 isoforms; therefore, it remains unknown if sM8 can influence TRPM8-mediated Ca^{2+} release from the endoplasmic reticulum.

It is also not clear whether sM8 isoforms have any significance independent of the full-size TRPM8 channel. Indeed, PCR screenings showed that some tissues express sM8 isoforms without classic TRPM8 (for instance, liver and breast). Therefore, it is quite plausible that, in addition to regulating full-size TRPM8, sM8 isoforms may have some additional physiological roles.

Acknowledgment—We thank Prof. Norman Scholfield for critical reading of the manuscript.

REFERENCES

1. Clapham, D. E. (2003) TRP channels as cellular sensors. *Nature* **426,** 517–524
2. Dhaka, A., Viswanath, V., and Patapoutian, A. (2006) Trp ion channels and temperature sensation. *Annu. Rev. Neurosci.* **29,** 135–161
3. Montell, C. (2005) The TRP superfamily of cation channels. *Sci. STKE* 2005, re3
4. Dragoni, I., Guida, E., and McIntyre, P. (2006) The cold and menthol receptor TRPM8 contains a functionally important double cysteine motif. *J. Biol. Chem.* **281,** 37353–37360
5. Strübing, C., Krapivinsky, G., Krapivinsky, L., and Clapham, D. E. (2001) TRPC1 and TRPC5 form a novel cation channel in mammalian brain. *Neuron* **29,** 645–655
6. Chu, X., Tong, Q., Wozney, J., Zhang, W., Cheung, J. Y., Conrad, K., Mazack, V., Stahl, R., Barber, D. L., and Miller, B. A. (2005) Identification of an N-terminal TRPC2 splice variant which inhibits calcium influx. *Cell Calcium* **37,** 173–182
7. Vázquez, E., and Valverde, M. A. (2006) A review of TRP channel splicing. *Semin. Cell Dev. Biol.* **17,** 607–617
8. Bidaux, G., Flourakis, M., Thebault, S., Zholos, A., Beck, B., Gkika, D., Roudbaraki, M., Bonnal, J. L., Mauroy, B., Shuba, Y., Skryma, R., and Prevarskaya, N. (2007) Prostate cell differentiation status determines transient receptor potential melastatin member 8 channel subcellular localization and function. *J. Clin. Invest.* **117,** 1647–1657
9. Oberwinkler, J., Lis, A., Giehl, K. M., Flockerzi, V., and Philipp, S. E. (2005) Alternative splicing switches the divalent cation selectivity of TRPM3 channels. *J. Biol. Chem.* **280,** 22540–22548
10. Fang, D., and Setaluri, V. (2000) Expression and up-regulation of alternatively spliced transcripts of melastatin, a melanoma metastasis-related gene, in human melanoma cells. *Biochem. Biophys. Res. Commun.* **279,** 53–61
11. Wehage, E., Eisfeld, J., Heiner, I., Jüngling, E., Zitt, C., and Lückhoff, A. (2002) Activation of the cation channel long transient receptor potential channel 2 (LTRPC2) by hydrogen peroxide. A splice variant reveals a mode of activation independent of ADP-ribose. *J. Biol. Chem.* **277,** 23150–23156
12. Zhang, W., Chu, X., Tong, Q., Cheung, J. Y., Conrad, K., Masker, K., and Miller, B. A. (2003) A novel TRPM2 isoform inhibits calcium influx and susceptibility to cell death. *J. Biol. Chem.* **278,** 16222–16229
13. Xu, X. Z., Moebius, F., Gill, D. L., and Montell, C. (2001) Regulation of melastatin, a TRP-related protein, through interaction with a cytoplasmic isoform. *Proc. Natl. Acad. Sci. U.S.A.* **98,** 10692–10697
14. Tsavaler, L., Shapero, M. H., Morkowski, S., and Laus, R. (2001) *Trp-p8*, a novel prostate-specific gene, is up-regulated in prostate cancer and other malignancies and shares high homology with transient receptor potential calcium channel proteins. *Cancer Res.* **61,** 3760–3769
15. McKemy, D. D., Neuhausser, W. M., and Julius, D. (2002) Identification of a cold receptor reveals a general role for TRP channels in thermosensation. *Nature* **416,** 52–58

16. Peier, A. M., Moqrich, A., Hergarden, A. C., Reeve, A. J., Andersson, D. A., Story, G. M., Earley, T. J., Dragoni, I., McIntyre, P., Bevan, S., and Patapoutian, A. (2002) A TRP channel that senses cold stimuli and menthol. *Cell* **108,** 705–715
17. Werten, P. J., Stege, G. J., and de Jong, W. W. (1999) The short 5′ untranslated region of the βA3/A1-crystallin mRNA is responsible for leaky ribosomal scanning. *Mol. Biol. Rep.* **26,** 201–205
18. Erler, I., Al-Ansary, D. M., Wissenbach, U., Wagner, T. F., Flockerzi, V., and Niemeyer, B. A. (2006) Trafficking and assembly of the cold-sensitive TRPM8 channel. *J. Biol. Chem.* **281,** 38396–38404
19. Voets, T., Droogmans, G., Wissenbach, U., Janssens, A., Flockerzi, V., and Nilius, B. (2004) The principle of temperature-dependent gating in cold- and heat-sensitive TRP channels. *Nature* **430,** 748–754
20. Brauchi, S., Orio, P., and Latorre, R. (2004) Clues to understanding cold sensation: thermodynamics and electrophysiological analysis of the cold receptor TRPM8. *Proc. Natl. Acad. Sci. U.S.A.* **101,** 15494–15499
21. Fernández, J. A., Skryma, R., Bidaux, G., Magleby, K. L., Scholfield, C. N., McGeown, J. G., Prevarskaya, N., and Zholos, A. V. (2011) Voltage- and cold-dependent gating of single TRPM8 ion channels. *J. Gen. Physiol.* **137,** 173–195
22. Fernández, J. A., Skryma, R., Bidaux, G., Magleby, K. L., Scholfield, C. N., McGeown, J. G., Prevarskaya, N., and Zholos, A. V. (2012) Short Isoforms of the Cold Receptor TRPM8 Inhibit Channel Gating by Mimicking Heat Action Rather than Chemical Inhibitors. *J. Biol. Chem.* **287,** 2963–2970
23. Brauchi, S., Orta, G., Salazar, M., Rosenmann, E., and Latorre, R. (2006) A hot-sensing cold receptor: C-terminal domain determines thermosensation in transient receptor potential channels. *J. Neurosci.* **26,** 4835–4840
24. Chuang, H. H., Neuhausser, W. M., and Julius, D. (2004) The super-cooling agent icilin reveals a mechanism of coincidence detection by a temperature-sensitive TRP channel. *Neuron* **43,** 859–869
25. Rohács, T., Lopes, C. M., Michailidis, I., and Logothetis, D. E. (2005) $PI(4,5)P_2$ regulates the activation and desensitization of TRPM8 channels through the TRP domain. *Nat. Neurosci.* **8,** 626–634
26. Vanden Abeele, F., Zholos, A., Bidaux, G., Shuba, Y., Thebault, S., Beck, B., Flourakis, M., Panchin, Y., Skryma, R., and Prevarskaya, N. (2006) Ca^{2+}-independent phospholipase A2-dependent gating of TRPM8 by lysophospholipids. *J. Biol. Chem.* **281,** 40174–40182
27. Andersson, D. A., Nash, M., and Bevan, S. (2007) Modulation of the cold-activated channel TRPM8 by lysophospholipids and polyunsaturated fatty acids. *J. Neurosci.* **27,** 3347–3355
28. Thebault, S., Lemonnier, L., Bidaux, G., Flourakis, M., Bavencoffe, A., Gordienko, D., Roudbaraki, M., Delcourt, P., Panchin, Y., Shuba, Y., Skryma, R., and Prevarskaya, N. (2005) Novel role of cold/menthol-sensitive transient receptor potential melastatin family member 8 (TRPM8) in the activation of store-operated channels in LNCaP human prostate cancer epithelial cells. *J. Biol. Chem.* **280,** 39423–39435